RSC Advances

PAPER

View Article Online
View Journal | View Issue

Cite this: *RSC Adv.*, 2024, **14**, 23286

Enhancing bioactivity and mechanical performances of hydroxyapatite–calcium sulfate bone cements for bone repair: *in vivo* histological evaluation in rabbit femurs

Pharatree Jaita, [abc] Komsanti Chokethawai,[a] Chamnan Randorn,[d] Kittikorn Boonsri, [e] Kidsadagon Pringproa,[f] Kriangkrai Thongkorn,[f] Anucha Watcharapasorn [ac] and Parkpoom Jarupoom [*gh]

This study deals with synthesizing hydroxyapatite–calcium sulfate bone cements or HAP–*x*CaS for bone repair. The effect of CaS on the setting time, injectability, washout resistance, phase evolution, water absorption, and physical, microstructural, and mechanical properties, as well as *in vitro* apatite-forming ability test and pH behavior of the HAP were investigated. Implantation of bone cement in rabbit femur and *in vivo* histological analysis were also analyzed. Initial and final setting times decrease with increasing CaS, which would be helpful for clinical procedures. All compositions have mixed phases of HAP, CaS, brushite, and gypsum. The prepared bone cement exhibited a dense structure and increased linear shrinkage with increasing CaS content. Adding more CaS inhibited grain growth and improved the mechanical properties, including compressive strength (σ_c), bending strength (σ_f), and Young's modulus (E). SEM micrographs displayed that the $x = 0.7$ or HAP–0.7CaS bone cement produced the highest ability to induce *in vitro* apatite formation, indicating its biocompatibility. *In vivo* histological analysis for the HAP–0.7CaS bone cement demonstrated that more new bone formed around defects and bone cement particles. Osteoblasts were found peripherally at the bone trabeculae, and occasional osteoblast-like cells were observed at the granules after 4–8 weeks of implantation. The obtained results indicated that the HAP–0.7CaS bone cement has the potential to exhibit good bioactivity, injectability, and good mechanical properties for bone repair applications.

Received 19th May 2024
Accepted 8th July 2024

DOI: 10.1039/d4ra03686g

rsc.li/rsc-advances

1 Introduction

Nowadays, many researchers have focused on bone cements due to their possible use in the restoration of bone defects.[1] Bone cement plays an important role in orthopedics and dentistry through minimally invasive procedures because of its injectability, moldability to fill irregularly shaped defects, self-setting ability, and low risk.[1–4] Moreover, bone cement transfers the load from the prosthesis to the bone and can be used as an implant coating for a bioactive substance.[5] Delivery of the cement through a needle or cannula will make it more useful in clinical applications.[1] Currently, many bone cements are being studied as bone substitute biomaterials for different pathologies. The search for bone substitutes with appropriate bioactivity and mechanical properties is still a research hotspot.[6,7]

Hydroxyapatite ($Ca_{10}(PO_4)_6(OH)_2$ or HAP) is one of the most widely used biomaterials in the field of biomaterials for bone substitutes and tissue engineering. HAP is a calcium phosphate-based material with a Ca/P ratio of ~1.67,[8] which shows structural and chemical similarities to the human bone skeleton.[9,10] It is a major mineral constituent of the bone matrix owing to its good biocompatibility with human tissues, bioactivity, and long-term stability in living tissues.[9–15] Many HAP applications in medicine include bone repair, dental uses, implant coating, and drug delivery systems.[11,16,17] HAP has excellent bioactivity; however, as a starting material for bone cement, HAP is not self-setting. Furthermore, HAP has a slow

[a]*Department of Physics and Materials Science, Faculty of Science, Chiang Mai University, Chiang Mai 50200, Thailand*
[b]*Office of Research Administration, Chiang Mai University, Chiang Mai 50200, Thailand*
[c]*Center of Excellence in Materials Science and Technology, Materials Science Research Center, Faculty of Science, Chiang Mai University, Chiang Mai 50200, Thailand*
[d]*Department of Chemistry, Faculty of Science, Chiang Mai University, Chiang Mai 50200, Thailand*
[e]*Center of Veterinary Diagnosis and Technology Transfer, Faculty of Veterinary Medicine, Chiang Mai University, Chiang Mai 50100, Thailand*
[f]*Faculty of Veterinary Medicine, Chiang Mai University, Chiang Mai 50100, Thailand*
[g]*Department of Industrial Engineering, Faculty of Engineering, Rajamangala University of Technology Lanna (RMUTL), Chiang Mai 50300, Thailand. E-mail: noteparkpoom@gmail.com*
[h]*Materials and Medical Innovation Research Unit, Faculty of Engineering, Rajamangala University of Technology Lanna (RMUTL), Chiang Mai 50300, Thailand*

resorption rate, slow degradation, and low mechanical performance, which limits its applications.[2]

Currently, calcium sulfate cement or CaS cement has been used extensively as a bioabsorbable bone substitute for over 100 years.[18–21] It is one of the most frequently used bone cement because of its desirable properties, such as self-setting, good biocompatibility, degradability, and rapidly and completely bioresorbable material.[22–25] Moreover, it is low cost and has an abundant supply.[26] Typically, calcium sulfate hemihydrate (CSH, $CaSO_4 \cdot 0.5H_2O$) mixed with water can undergo *in situ* setting and transform into calcium sulfate dihydrate or gypsum ($CaSO_4 \cdot 2H_2O$), which is in the hard cement form.[27,28] The properties of cements can be improved by manipulating their chemical composition, changing the particle size of initial powders, using various types of liquid phases with different liquid-to-powder ratios and introducing various additives.[29]

Hao *et al.*[3] studied the calcium sulfate–tricalcium silicate (CS/C3S) composite cement. They reported that incorporating C3S could be a feasible approach to improve the biological performance of CS-based bone cement as a biodegradable implant for bone repair in clinical applications. Chen *et al.*[30] found that the mineralized collagen/calcium sulfate hemihydrate (*n*HAC/CSH) composite is an injectable bone repair material with controllable injectability and self-setting properties prepared by introducing CSH into *n*HAC. These composites have good biocompatibility and osteogenic capability. A mixture of $CaSO_4 \cdot 1/2H_2O$ and hydroxyapatite (HAP) with varying liquid/powder ratios from 0.4–1.8 was prepared by Cabaňas *et al.*[31] They reported that the biphasic specimens had apparent densities slightly higher than those of a pure phase. The incorporation of 40 wt% of HAP showed an improvement in the bioactivity response when compared to pure HAP or gypsum when soaked in simulated body fluid (SBF). Yang *et al.*[32] prepared calcium sulfate/magnesium phosphate cement composite (CSMPC). They reported that the prepared CSMPC composites featured the controllable setting time mechanical strength and degradation rate by adjusting MPC, which would provide the facility to fulfill the requirement for the clinical application. The CSMPCs also exhibited excellent bioactivity and good biocompatibility to enable the cells to attach to and proliferate on the surface. This CSMPC composite has the potential to serve as a bone graft for bone regeneration.

The compounds of HAP and CaS are very interesting, and both are commonly used to fill bone defects in clinical trials.[33] The HAP has good biocompatibility and bone conductivity, which can be in close contact with bone tissue and induce new bone formation,[34–36] while the CaS has excellent self-setting properties, good biocompatibility, degradability, and rapidly and completely bioresorbable material.[1,37] Consequently, attempts to combine the advantages of HAP and CaS compounds were then carried out.

In this work, we attempt to synthesize the HAP–*x*CaS bone cements for bone repair. To reduce the raw chemical substance at a low cost for the final product, the studied HAP powder in this work was synthesized from bovine bone, which is a natural material and a waste product. This method is easy and quick to prepare. Moreover, the yield product from natural materials is very high when compared to that of chemical techniques (high cost and low yield). Considering the consolidation ability of CaS and the biocompatibility of the HAP, the two materials are mixed to complement each other. The effect of CaS content on the initial and final setting times, phase, physical, water absorption, microstructure, and mechanical properties of HAP was investigated. Moreover, we investigated *in vitro* apatite-forming ability and pH behavior in SBF at 37 °C of the HAP–*x*CaS bone cements. Furthermore, the effect of material implantation in rabbit femur and *in vivo* histological analysis are investigated and discussed in detail. These properties are essential for evaluating the availability of biomaterials in guiding tissue regeneration and repair.[28] In this work, the formation of new bone tissue with good bioactivity was also demonstrated. We also demonstrated that the HAP–*x*CaS bone cement composites have good liquidity, injectability, and biocompatibility[38] compared to a single HAP or CaS, suggesting their potential use for bone repair applications.

2 Experimental

2.1 Synthesis of the nano-hydroxyapatite powder from the natural bovine bone

The hydroxyapatite [$Ca_{10}(PO_4)_6(OH)_2$ or HAP] powder was derived from the natural bovine bone by a sequence of thermal processing. The fresh bovine bones of a cow were cut and cleaned well to remove visible adhering impurities and substances, which included the ligaments and tissues stuck on the bone. The clean bone was defatted by boiling it in distilled water to remove the bone marrow and tendons for 8 h. Then, the bovine bone is deproteinized by continued boiling in water. The boiled bone samples were then dried overnight at 200 °C. Next, the deproteinized bone was calcined at 800 °C for 3 h dwell time with a heating/cooling rate of 3 °C min^{-1}. After that, it was coarse ground with a mortar.[36] To obtain the nano-powder, the HAP was then milled by applying a high-energy vibro-milling method for 20 min. In addition, the particle size distribution of the HAP nano-powder powder was examined using a dynamic light scattering technique (DLS, Zetasizer [Nano Series]). A schematic of the methods used to fabricate the HAP nano-powder is shown in Fig. 1.

Fig. 1 Schematic of methods to fabricate the nano hydroxyapatite (HAP) powder.

2.2 Preparation of the hydroxyapatite–calcium sulfate bone cements (HAP–*x*CaS)

Calcium sulfate hemihydrate (CSH) with medicine grade was the raw material obtained from Merck & Co., Inc. (Germany). The CSH can react with water immediately and transform into CaS or $CaSO_4 \cdot 2H_2O$, which is in the form of solid and hard cement.[27,28] The HAP nano-powder was derived from the natural bovine. The resulting HAP and CaS powders were weighed and mixed to obtain the mixed powder of HAP–*x*CaS, where $x = 0$–1 weight fraction. XRD was performed on the mixed powders for phase identification. To obtain the bone cement, each of the mixed powders was individually mixed with deionized water at a powder-to-liquid ratio of 2 : 1, which was mixed well using a spatula. The cement was quickly transferred to a mold (with bar or cylindrical), as shown in Fig. 2. The HAP–*x*CaS samples were placed in a water bath with 100% humidity and a temperature of 37 °C until the setting steps were completed.[39] After that, all HAP–*x*CaS bone cements were then characterized.

2.3 Injectability, washout resistance, and setting time tests

The injectability test was evaluated by extruding the cement paste through a disposable syringe. The washout resistance test of the injected HAP–*x*CaS cement paste was also measured. Briefly, each HAP–*x*CaS cement paste was placed in a syringe (5 mL) with an opening nozzle diameter of 2.0 mm[40] and injected into Ringer's solution at 37 °C. After that, the weight loss of cement paste (%) after immersion of 0, 5, 10, 15, 20, 25, and 30 minutes in the Ringer's solution was also measured. Normally, it was assumed to pass the washout resistance test if the paste did not dissociate in the Ringer's solution after 30 minutes of immersion and showed a minimum weight loss of cement paste.

For setting time test, the HAP–*x*CaS samples were prepared as described earlier and checked from time to time using a testing apparatus. The setting time of each HAP–*x*CaS sample was tested using a 400 G Gillmore needle with a 1 mm diameter according to ISO 9917-1 for water-based cement. The initial setting time was defined as the point when a needle with a 1 mm diameter failed to create an indentation of 1 mm in depth on the surface of the specimen with a load of 300 g in three separate areas. The final setting time was defined as the time that elapsed until the needle failed to penetrate or produce flaws on the surface of the specimens.[39] The setting time of six specimens for each cement group was measured, and the results were expressed as mean ± SD.[40]

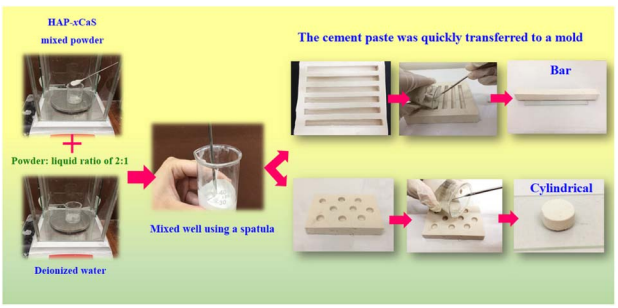

Fig. 2 Schematic of methods to prepare the HAP–*x*CaS bone cements with different shapes.

2.4 Phase evaluation

X-ray diffraction (XRD, Rigaku, MiniFlex 600) was used for the phase identification of the HAP powder, the mixed powders of HAP–*x*CaS, and the HAP–*x*CaS bone cements. The source of the X-ray was CuKα radiation (wavelength of 1.5405 Å) with the tube voltage and current of 35 kV and 30 mA, respectively. Room temperature XRD data was recorded in 2θ between 10 and 60° with a step size of 0.02° s^{-1}. The quantitative phase composition (%) of the HAP–*x*CaS bone cements was analyzed by applying the Reference Intensity Ratio (RIR) method using the SmartLab Studio II program.

2.5 Physical properties and water absorption analysis

The bulk density and porosity measurements were conducted using a liquid displacement technique. This work used ethanol as the displacement liquid because water was the setting liquid. Before the measurement, the bone cement samples were dried in an oven at 120 °C for 2 h. The sample was immersed in a graduated cylinder containing a known volume (V_1) of ethanol. Afterward, it was ultrasonically stirred for at least 3 min to force the ethanol into the pores of the specimens until no air bubbles were observed emerging from the sample. The total volume of ethanol and the ethanol-impregnated sample was then recorded as V_2. The ethanol-impregnated sample was removed from the cylinder, and the residual ethanol volume was recorded as V_3. The volume differences, $(V_1 - V_3)$ and $(V_2 - V_3)$, were the pore and total volumes, respectively. Thus, the porosity of the sample was obtained using the following equation:[28]

$$\text{Porosity} = (V_1 - V_3)/(V_2 - V_3) \times 100\%. \quad (1)$$

The water absorption and rate of absorption values were calculated in this study. The linear shrinkage value was also calculated using the following empirical equation:[41]

$$S_L = [(D_1 - D_2)/D_1] \times 100\%, \quad (2)$$

where S_L (%) is the linear shrinkage, D_1 (mm) is the length of the mold, and D_2 (mm) is the length of the sample after the completed setting.

2.6 Microstructural analysis

First, the samples were cleaned with an ultrasonic cleaner and then fixed on a brass stub. All samples on the stub were coated with gold sputtering (JFC-1100E). A scanning electron microscope (SEM, Prisma E Microscope, Thermo Fisher Scientific, USA) was used to study the microstructural features of the HAP–*x*CaS bone cements. During image acquisition, the secondary electron modes were utilized with an accelerating voltage of 15 kV. The grain size of all bone cements was determined using the linear intercept method (ASTM no. E112-88). This method was

the quantitative measurement of grain size values within a dense uniform structure, and it was the best suited where the boundaries of each grain were relatively easy to determine.[42]

2.7 Mechanical properties

In this research, the compressive strength (σ_c) of all samples was measured following ASTM C773-88(1999) to evaluate their structural integrity[43] using a universal testing machine (Hounsfield, H50KS) with a cylinder specimen size of 10 mm in length and 5 mm in diameter. The top and bottom surfaces were loaded at a 5 mm min^{-1} crosshead speed using a screw-driver load frame. The σ_c of each sample was calculated using the following equation:

$$\sigma_c = \frac{P}{A}, \quad (3)$$

where σ_c is the compressive strength (MPa), A is the calculated area of the bearing surface of the sample (mm^2), and P is the total load on the sample at failure (N). In addition, the σ_c values after 1, 3, and 7 days of incubation were measured in this work.

The bending strength or flexural strength (σ_f) was also studied in this work using a universal testing machine (Hounsfield, H50KS), following the method described by ASTM C 1161-94(1996). Five samples with rectangular specimen dimensions of 8 × 6 × 100 mm were designed, and the average results were reported.[44] The σ_f of each sample was determined using the following formula:

$$\sigma_f = \frac{3PL}{2bd^2}, \quad (4)$$

where σ_f is bending strength (MPa), L is the length of the support span, P is the load (force) at the fracture point (N), d is the thickness, and b is the width. The Young's modulus (E) value was also calculated using the following equation:

$$E = \frac{L^3P}{4bd^3Y}, \quad (5)$$

where E is Young's modulus (MPa), L is the length of the support span, P is the load (force) at the fracture point (N), d is the thickness, b is the width, and Y is the bending distance of the test sample.

2.8 Statistical analysis

For statistical analysis, the results were then analyzed using simple statistical analysis, which is an analysis of variants (ANOVA) at a significance level of 5% ($P < 0.05$) to determine the statistical significance of the data.[38] Results were expressed as mean ± standard deviation (SD).[25,45,46]

2.9 *In vitro* apatite-forming ability test and pH behavior

For the *in vitro* apatite-forming ability test, the HAP–xCaS bone cements were placed in a mold with 5 mm in diameter and 10 mm in height to make a cylindrical shape and incubated at 37 °C in a saturated 100% humidity environment.[25] The studied samples were immersed in simulated body fluid solution (SBF) and incubated at 37 °C for 7 and 14 days. The SBF solution is the closest to human plasma. The ionic concentration of SBF (in mM) was the following: $Na^+ = 142.0$, $K^+ = 5.0$, $Ca^{2+} = 2.5$, $Mg^{2+} = 1.5$, $Cl^- = 148.8$, $HCO_3^- = 4.2$, $HPO_4^{2-} = 1.0$, and $SO_4^{2-} = 0.5$.[42,47] The SBF solution was changed every 1 h for up to 12 h, followed by replacement with fresh solution once a day for 14 days. For each time point, pH changes were recorded using a pH-meter (Thermo Fisher Scientific, USA).[25] After 7 and 14 days of soaking in SBF, the samples were investigated for apatite-forming ability by applying SEM techniques.

2.10 *In vivo* studies

2.10.1 Animal implantation of hydroxyapatite–calcium sulfate bone cements. The animal study was approved by the Faculty of Veterinary Medicine, Chiang Mai University, Thailand (Animal Use Protocol Ref. No. R16/2559). Six adult male New Zealand white rabbits (12 week-old) weighing 3 kg each were chosen for the *in vivo* investigation or implant of the HAP–xCaS bone cement. First, rabbits were intramuscularly injected with xylazine 5 mg kg^{-1} combined with Zoletil® 15 mg kg^{-1} as general anesthesia. The subcutaneous analgesic (tramadol 4 mg kg^{-1}) and subcutaneous antibiotics (enrofloxacin 5 mg kg^{-1}) were injected. The anesthesia was maintained with isoflurane 1–2%. The defect sites were created using a trephine drill with two holes at the center of each femoral bone axis 5 mm in diameter and 10 mm in depth, approximately 2.5 cm apart. The HAP–CaS bone cements (cylinder specimen size of 5 mm in diameter and 10 mm in length) were placed into the defect sites, and the adjacent soft tissue was then sutured to secure the test material at the defect sites. After 2, 4, and 8 weeks, the rabbits were sacrificed, and the en bloc femoral diaphysis was obtained for *in vivo* histological analysis.[3,20,48]

2.10.2 Histological analysis. The en bloc femoral diaphysis of rabbit femurs at the surgical sites was collected and fixed in a 10% neutral buffered formalin solution at room temperature. Each sample was decalcified with 4% nitric acid and dehydrated using an alcohol series. Residual alcohol was removed by immersion in xylene, and the tissue sample was embedded in a paraffin block. Tissue slices (5 μm thick) were cut using a microtome and stained with hematoxylin and eosin (H&E) and Masson's trichrome stains. The sections were observed using a model BX53 microscope (Olympus, Japan) and photographed with an Olympus DP72 camera. Images were analyzed using Cellsens software (Olympus).[3,48,49]

3 Results and discussion

3.1 Structure and dynamic light scattering analysis of the HAP

X-ray diffraction patterns of the HAP nano-powder synthesized from the natural bovine bone (calcined @ 800 °C for 3 h) are shown in Fig. 3a. XRD data were recorded in the range of 2θ = 20–60°, with a step size of 0.02° s^{-1}, using CuKα radiation at 35 kV, and 30 mA with $\lambda = 1.5405$ Å. Based on the XRD analysis, a pure phase of the HAP was successfully obtained. The XRD data were found to match the stoichiometric of hydroxyapatite

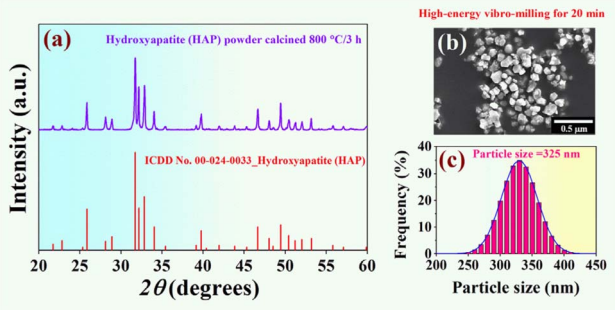

Fig. 3 (a) X-ray diffraction patterns of the nano HAP powders calcined at 800 °C for 3 h where $2\theta = 20–60°$, (b) SEM micrograph of the nano HAP powder prepared by high-energy vibromilling technique for 20 min, and (c) particle size distribution histogram of the nano HAP powder.

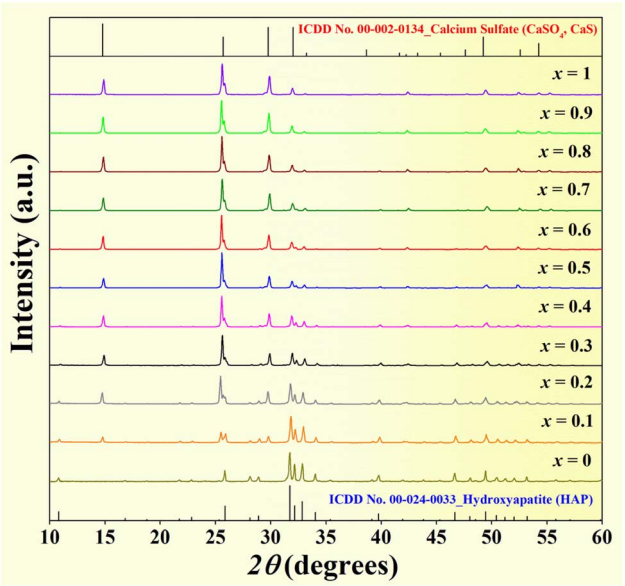

Fig. 4 X-ray diffraction patterns of the HAP–xCaS mixed powder (x = 0–1), where $2\theta = 10–60°$.

$Ca_{10}(PO_4)_6(OH)_2$, which correlated with ICDD data file no. 00-024-0033 in a hexagonal single phase.[50,51] SEM micrograph of the HAP nano-powder was prepared by applying a high-energy vibro-milling technique for 20 min, as shown in Fig. 3b. The particles of the HAP nano-powder synthesized from the natural bovine bone showed a small size with a round shape.

The dynamic light scattering (DLS) technique was used to examine the particle size distribution of the HAP nano-powder,[52] and the result is shown in Fig. 3c. It was found that the powder preparation technique for the particle size analysis in this work was used to prepare a well-dispersed particle. Therefore, there are no traces of particle agglomeration. The particle size distributions showed a mono-modal distribution.[53] As estimated from the particle size analysis, the average particle size of the HAP nano-powder was 325 nm. Furthermore, the particle size ranged from 230 to 430 nm. This means that our processing can produce the nano-powder particle sizes of HAP.[36]

X-ray diffraction patterns of the mixed powder HAP–xCaS (x = 0–1), where $2\theta = 10–60°$, are shown in Fig. 4. The pure HAP powder had a hexagonal phase according to ICDD data file no. 00-024-0033,[42,50,51] while the pure CaS matched with ICDD file no. 00-002-0134. This was also consistent with the previous work.[54] By increasing the CaS content, the main peak of the CaS phase was dominantly observed. Except for the pure HAP and the pure CaS, all compositions showed two-phase mixture peaks of HAP and CaS with intensities corresponding to the relative amount of each phase.

3.2 Setting time, injectability, and washout resistance

The significant advantage of bone cement is its self-setting ability at body temperature when injected into the defect site.[48,55] However, the setting reaction and hardening time of *in situ* bone cement vary depending on many factors. Chemical composition, particle size, and liquid phase, as well as the ratio of liquid to powder play a crucial role in the setting time of cement materials.[28] Therefore, each composition of bone cement must be optimized to control the setting reaction.[48] Setting time is one of the most clinically relevant factors, and a long setting duration could cause clinical problems due to the cement's inability to maintain shape and support stress during this period.[28] Generally, self-setting bone cement should react slowly enough to allow enough time for the surgeon to implant it and fast enough to prevent delays in surgery. Good mechanical properties should also be reached within minutes after the initial setting.[39,56] In this work, the initial and final setting times were measured depending on the CaS content. It was noted that the composition of x = 0–0.2 could not be set to the solid and hard bone cements, while the composition of x = 0.8–1.0 was too viscous, and the cement paste of these compositions could not be injected or extruded through a disposable syringe. Therefore, the x = 0–0.2 and the x = 0.8–1.0 samples were excluded from further investigations and characterizations.

Plots of the initial setting time and final setting time values as a function of the CaS content of the HAP–xCaS bone cements, where x = 0.3–0.7, are shown in Fig. 5a, and the related values are also summarized in Table 1. The setting time testing apparatus is also shown in the inset of Fig. 5a. Usually, a standard for setting time in clinical use is that the initial setting time should range from 3 to 8 min. The setting time of cement generally corresponds to the onset of the setting reaction. Therefore, the setting time depends on the initial setting rate of the cement. The setting rate of the cement is not a constant value but varies with time. A particular cement might have a short setting time but might require a long time to reach complete conversion.[39] Based on Fig. 5a and Table 1, the setting time value was reduced by adding CaS. The initial and final setting times further decreased with the increase in the CaS content and showed the minimum values for the x = 0.7 bone cement. The x = 0.7 sample displayed the fastest reaction among all samples with the minimum initial and final setting times of 8.04 ± 0.15 min and 23.25 ± 0.34 min, respectively.

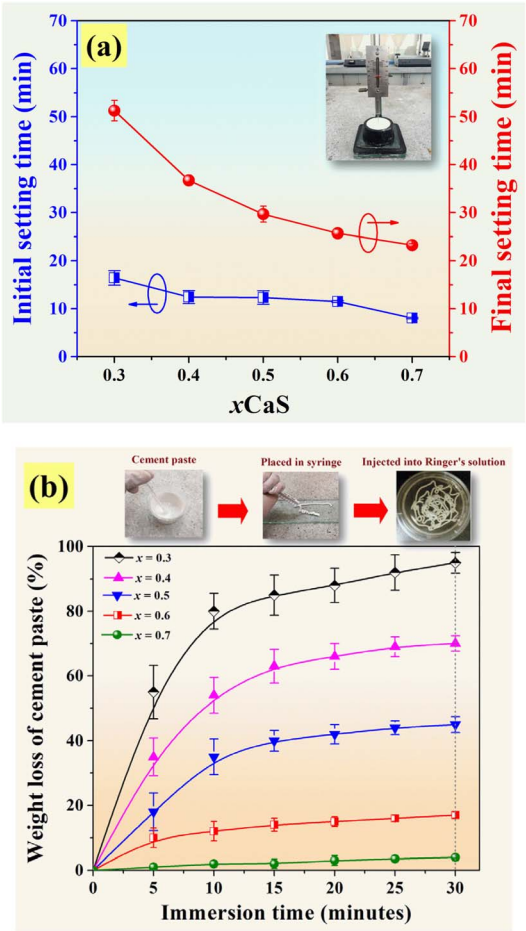

Fig. 5 Plots of (a) the initial setting time and final setting time as a function of CaS content, and (b) the weight loss of cement paste (%) after immersion in the Ringer's solution as a function of immersion time (inset: pictures showing the injectability and washout resistance tests).

Therefore, the $x = 0.7$ sample had good initial and final setting times, and we expected that the $x = 0.7$ bone cement should be appropriate for bone repair application. It was also demonstrated that a significant reduction in setting time would be helpful for clinical procedures; normally, an average initial setting time of about 20 min is considered optimum for dental implants.[57]

Another important factor in handling the HAP–xCaS cement pastes was their injectability.[48] Normally, injectability can be defined as the ability of a cement paste to extrude through the syringe. During injection, the extruded paste must maintain homogeneity. This is a key element in the development of injectable bone cements. The literature has no unified standard procedure for measuring injectability. Usually, it is identified by the force required for the complete extraction or quantification of extruded material during a certain period.[58] For the present work, injectability was evaluated by extruding the cement paste through a disposable syringe according to a modified method described in the experimental part.[59] Generally, the rheological properties of the bone cement should be sufficient to allow injection through the needle at a force that a surgeon can apply to fill the fracture site. Additionally, the bone cement should have sufficient cohesion to prevent disintegration in the body.[48] Bone cement without additives typically has poor injectability due to its lower cohesion properties.[60] This poor cohesion renders the bone cement more prone to disintegration when the cement contacts blood or other biological fluids during the operation. This can lead to cement embolism with potentially fatal consequences.[48,61]

In this work, injectability, and washout resistance were also tested. The HAP–xCaS cement pastes were directly injected into Ringer's solution, and the weight loss of cement paste (%) after immersion in the Ringer's solution 0, 5, 10, 15, 20, 25, and 30 minutes was also measured. It was found that each composition of cement paste could be extruded through the syringe with homogeneity. Normally, if the paste did not dissociate in the Ringer's solution after 30 minutes of immersion and showed a minimum weight loss of cement paste, it was assumed to pass the washout resistance test. The weight loss of cement paste (%) after immersion in the Ringer's solution as a function of immersion time is shown in Fig. 5b. Based on Fig. 5b, the weight loss of cement paste was further increased with an immersion time ranging from 0 to 30 minutes. After 30 minutes of immersion, the $x = 0.3$ cement paste could not pass the washout resistance test because it was significantly dispersed in Ringer's solution and showed a high weight loss of cement paste value of 95.41 ± 3.23% (see Table 1). However, the $x = 0.4$–0.7 samples can pass the washout resistance test. The $x = 0.4$–0.6 cement pastes showed the weight loss of cement paste from around 17.25 ± 1.22 to 70.24 ± 2.44%, and the pastes were

Table 1 Setting time, weight loss of cement paste, and XRD analysis by SmartLab Studio II program of the HAP–xCaS samples

x	Initial setting time (min)	Final setting time (min)	Weight loss of cement paste[a] (after 30 min immersion) (%)	Phase composition[b] (%) (by RIR method)			
				HAP	Gypsum	Brushite	CaS
0.3	16.42 ± 1.52	51.28 ± 2.15	95.41 ± 3.23	46.90	30.19	22.90	0.01
0.4	12.43 ± 1.35	36.72 ± 1.05	70.24 ± 2.44	36.47	41.58	21.94	0.01
0.5	12.31 ± 1.41	29.67 ± 1.65	45.44 ± 2.51	30.31	48.32	21.35	0.02
0.6	11.50 ± 0.20	25.70 ± 0.85	17.25 ± 1.22	27.63	54.76	17.60	0.01
0.7	8.04 ± 0.15	23.25 ± 0.34	4.11 ± 0.91	21.81	64.34	13.82	0.03

[a] Weight loss of cement paste (%) after 30 minutes immersion in the Ringer's solution. [b] Phase composition of the HAP–xCaS bone cements analyzed by the Reference Intensity Ratio (RIR) method using SmartLab Studio II program.

maintained of some particles. The $x = 0.7$ sample exhibited a minimum weight loss of cement paste value, and the particles did not disintegrate and retained their original shape. Therefore, we can conclude that the $x = 0.7$ or HAP–0.7CaS sample had good injectability and washout resistance because the starch did not dissociate in the solution and showed a minimum weight loss of cement paste value of $4.11 \pm 0.91\%$.[48]

3.3 Phase evolution of the HAP–*x*CaS bone cements

Mixing HAP and CaS dry powders with liquid phase induced various chemical transformations. The XRD patterns of the studied bone cement made from mixtures of HAP and CaS with different ratios of HAP and CaS after being hardened at 37 °C for 24 h at 100% relative humidity are presented in Fig. 6. The XRD results revealed that all compositions contained multi-phases, including HAP, CaS, brushite, and gypsum. The quantitative analysis of each phase was thoroughly conducted using the Reference Intensity Ratio (RIR) method with the SmartLab Studio II program. The percentage of each phase composition (*i.e.* HAP, CaS, brushite, and gypsum) is depicted in Fig. 6 and Table 1. Based on Table 1, it was found that the $x = 0.3$ bone cement has the main phase of HAP (46.9%) with a small phase of CaS (0.01%). The XRD patterns also presented other phases, including calcium sulfate dihydrate or gypsum ($CaSO_4 \cdot 2H_2O$) at 30.19%, marked as "•", and dicalcium phosphate dehydrate (DCPD, $CaHPO_4 \cdot 2H_2O$) at 22.90%, marked as "*".[48,62,63] The DCPD also known by the mineral name of brushite crystallizes in the monoclinic structure. Generally, after the cementing reaction, the calcium sulfate hemihydrate ($CaSO_4 \cdot 0.5H_2O$) mixed with water to form the paste can undergo an *in situ* setting mechanism because $CaSO_4 \cdot 0.5H_2O$ can react with water (H_2O) immediately and transform into calcium sulfate dihydrate or gypsum ($CaSO_4 \cdot 2H_2O$), which is in the form of solid and hard lump cement within a restricted period.[27] The gypsum is chemically and crystallographically similar to brushite and a relatively soluble calcium-rich phase.[29] The formation of brushite as a by-product is possibly thought to result from the amount of Ca^{2+} (from $CaSO_4$) and $H_2PO_4^-$ (from $Ca_{10}(PO_4)_6(OH)_2$) ions in the system. Among the raw materials for preparing bone cement in this work, the $CaSO_4$ was acidic. As is known to all, the HAP with a higher Ca/P ratio (~1.67)[8] can dissolve under acid conditions and release out ions.[38] When pH in the system slightly decreases, the formation of brushite is expected.[29,38,62] The prominent presence of brushite peaks in this work was observed around 11.79°, 20.90°, and 29.29° created from the liquid and solid phase reaction.[29,48] Moreover, gypsum and brushite cement can have high binding properties, biological compatibility with living tissues, and a resorption rate.[64] Furthermore, the amount of the HAP phase was found to decrease while the gypsum phase increased as the CaS concentration increased, especially for the $x = 0.7$ bone cement. The gypsum phase was most prominent at 64.34%, and the HAP phase decreased to 21.81%. All bone cement compositions showed the mixture phases of HAP, CaS, brushite, and gypsum with the percentage of phase composition corresponding to the relative amount of each phase (see Table 1).

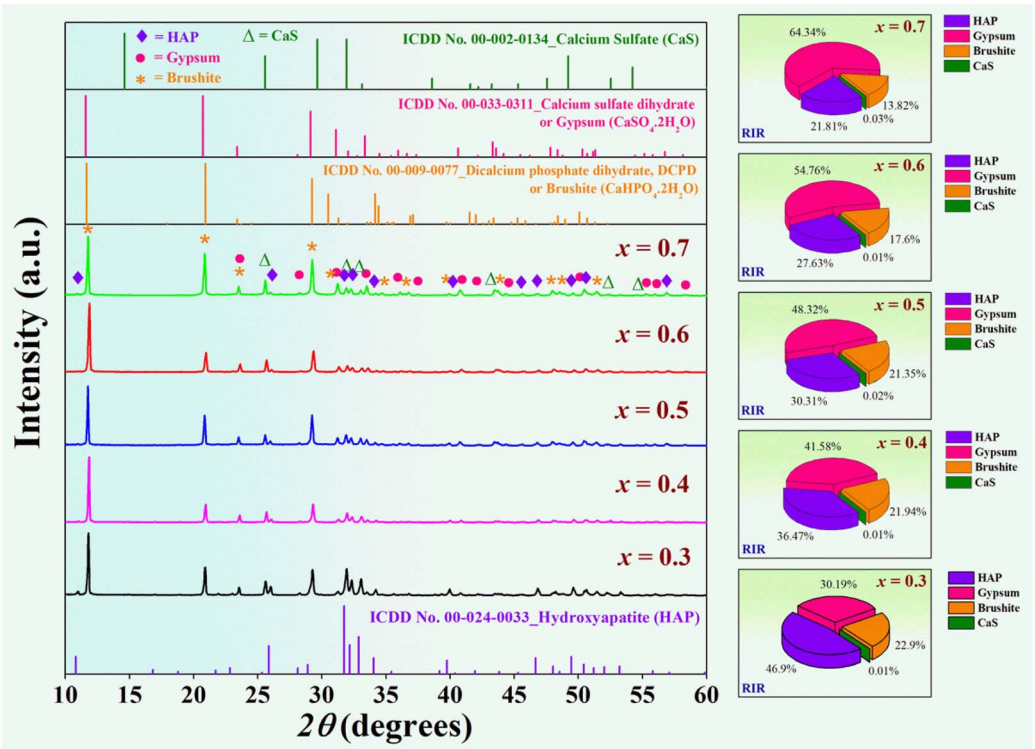

Fig. 6 X-ray diffraction patterns of the HAP–*x*CaS bone cements, where $2\theta = 10$–60° and phase composition (%) analyzed by the Reference Intensity Ratio (RIR) method using SmartLab Studio II program.

3.4 Physical properties and water absorption

The bulk density and porosity measurements were conducted using a liquid displacement technique to obtain the densest ceramic for each composition. Plots of the density value as a function of the CaS content of the HAP–*x*CaS bone cements are shown in Fig. 7a, and the value is listed in Table 2. The density tended to increase with CaS content and ranged from 1.25 ± 0.01 to 1.30 ± 0.02 g cm^{-3}. A maximum density of 1.30 g cm^{-3} was observed for the $x = 0.7$ bone cement. This result was also correlated with the increasing linear shrinkage value (calculated from eqn (2))[41] with increasing CaS additive, as shown in Fig. 7b and Table 2. The maximum linear shrinkage of 7.33 ± 0.11% was also obtained for the $x = 0.7$ bone cement. However, the trend of porosity, water absorption, and rate of absorption exhibited an opposite direction to the density and linear shrinkage results (Fig. 7c and d). The porosity, water absorption, and rate of absorption decreased with increased CaS content. They showed a minimum value of porosity (44.40 ± 0.09%), water absorption (23.07 ± 0.17%), and rate of absorption (5.15 ± 0.04 mm min^{-1}) for the $x = 0.7$ bone cement sample. The porosity of the $x = 0.7$ sample in this work was close to the porosity value of the HAP + Mg/CSH bone cement (~44–46%) observed previously by Zima *et al.*[29] These results suggested that the $x = 0.7$ or HAP–0.7CaS bone cement had the highest density and hence lowest porosity and lowest water absorption values. This result was also consistent with the previous work studied by Nagrockienė *et al.*[65] They also reported that when silica fume filled in small voids in concrete structures, it became more homogeneous, and the density increased, whereas the porosity and water absorption values decreased.

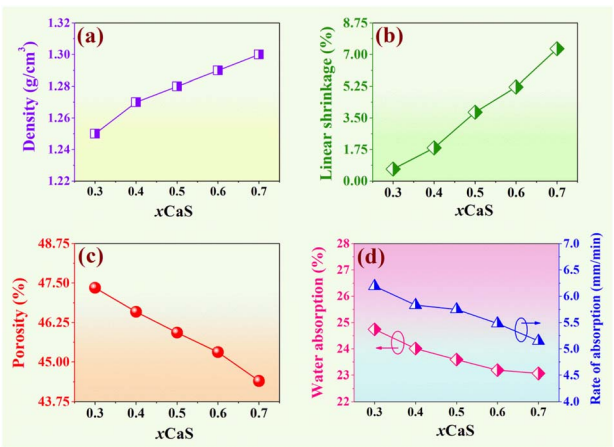

Fig. 7 Plots of (a) density, (b) linear shrinkage, (c) porosity, and (d) water absorption and rate of absorption as a function of CaS content of the HAP–*x*CaS bone cements.

3.5 Microstructural

Fig. 8a–e displays the surface mode of the studied bone cement samples using SEM. The microstructure of bone cement with different compositions showed a significant variation in grain morphology. The average grain size as a function of CaS content is shown in Fig. 8f, and the value is summarized in Table 3. Microstructural analysis indicated that increasing the CaS content decreased the average grain size value. The grain size decreased from 1.29 ± 0.02 μm for the $x = 0.3$ bone cement to around 1.22 ± 0.01 μm for higher amounts of CaS ($x = 0.5$) and then slightly decreased to the minimum value of around 1.19 μm for the $x = 0.7$ bone cement sample. Therefore, the grain size of the studied ceramics could be controlled by the CaS addition. The surface of the $x = 0.3$ bone cement sample showed a porous structure with coarser grain. By increasing the CaS content, the SEM images showed a finer grain and denser microstructure. This result also agrees well with the measured density result, *i.e.* the density increased and the porosity values decreased with CaS content.

3.6 Mechanical properties

Mechanical performance is also important for some biomaterial applications. Hence, it is necessary to produce a biomaterial with good mechanical properties. As it relates to biomaterial, the mechanical evaluations are of interest, including compressive strength, hardness, Young's modulus, fracture toughness, and brittle index.[66] In this work, the compressive strength (σ_c), bending strength or flexural strength (σ_f), and Young's modulus (E) were investigated using a universal testing machine. The σ_c, σ_f, and E values were calculated using empirical eqn (3)–(5), respectively, and the data are summarized in Table 3. Plots of σ_c and σ_f as a function of the CaS content of the HAP–*x*CaS bone cements are shown in Fig. 9a and b, respectively. The $x = 0.3$ bone cement had the σ_c of 3.06 ± 0.32 MPa and σ_f of 1.76 ± 0.31 MPa. The σ_c and σ_f values tend to increase as the CaS additive increases. The $x = 0.7$ bone cement showed the maximum values of both σ_c (7.23 ± 0.14 MPa) and σ_f (4.79 ± 0.16 MPa). It should be noted that the σ_c value of the $x = 0.7$ bone cement in this work was close to σ_c value of the HAP cement with 1–2% $NaH_2PO_4 \cdot 2H_2O$ (~5.0–6.0 MPa) observed

Table 2 Physical properties and water absorption of the HAP–*x*CaS bone cements

x	Density (g cm^{-3})	Porosity (%)	Linkage shrinkage (%)	Water absorption (%)	Rate of absorption (mm min^{-1})
0.3	1.25 ± 0.01	47.35 ± 0.14	0.67 ± 0.07	24.74 ± 0.22	6.19 ± 0.02
0.4	1.27 ± 0.02	46.59 ± 0.15	1.85 ± 0.10	24.01 ± 0.14	5.83 ± 0.04
0.5	1.28 ± 0.01	45.93 ± 0.08	3.82 ± 0.09	23.59 ± 0.12	5.75 ± 0.06
0.6	1.29 ± 0.01	45.31 ± 0.17	5.22 ± 0.13	23.19 ± 0.17	5.48 ± 0.03
0.7	1.30 ± 0.02	44.40 ± 0.09	7.33 ± 0.11	23.07 ± 0.17	5.15 ± 0.04

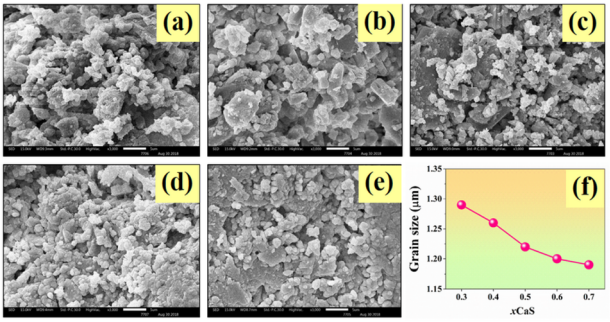

Fig. 8 SEM micrographs with surface mode of the HAP–*x*CaS bone cements, where (a) $x = 0.3$, (b) $x = 0.4$, (c) $x = 0.5$, (d) $x = 0.6$, (e) $x = 0.7$, and (f) plot of grain size as a function of CaS content.

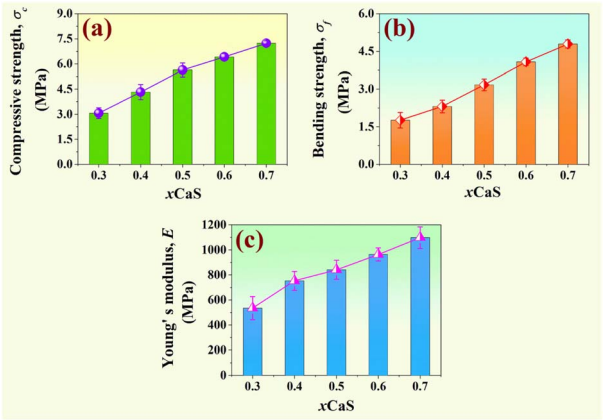

Fig. 9 Plots of (a) compressive strength (σ_c), (b) bending strength (σ_f), and (c) Young's modulus (E) as a function of CaS content of the HAP–*x*CaS bone cements.

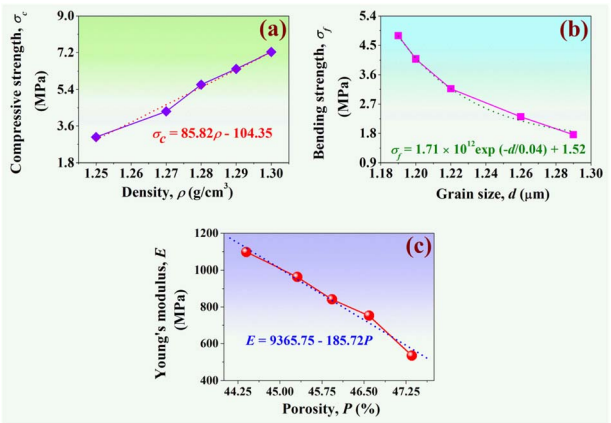

Fig. 10 Plots of (a) σ_c as a function of density (ρ), (b) σ_f as a function of grain size (d), and (c) E as a function of porosity (P) of the HAP–*x*CaS bone cements.

earlier by Rabiee *et al.*[13] Subramaniam *et al.*[57] also reported that the σ_c of hydroxyapatite/calcium sulfate hemihydrate/hyaluronic acid laden collagenase (HAP/CS/HA-Col) was around 6.69 ± 0.52 MPa.

The E value also showed a similar trend to the σ_c and σ_f values. The E value increased as the CaS content increased and exhibited the maximum value of 1097.48 ± 85.56 MPa for the $x = 0.7$ bone cement (Fig. 9c). These mechanical results were also correlated with an increase in density, linear shrinkage, and a decrease in porosity (Fig. 7a–c). Normally, the mechanical improvement depends on many factors, such as phase composition, type of materials, densification, porosity, and average grain size. In the present work, an improvement in mechanical properties in bone cement with a higher CaS additive concentration is likely due to the effect of the reduced average grain size, densification improvement, and reduction of porosity value.[67] Pineda *et al.*[68] reported that the incorporation of HAP into bone cement formulations can enhance the biocompatibility and bioactivity of the materials but generally reduce their mechanical properties. However, for this work, the mixing of HAP and CaS in a suitable composition can improve the mechanical properties of the bone cement. The development of materials with good mechanical properties without any effect on biological compatibility has become a significant and very important subject presently.

The relationship between the σ_c and the density (ρ) is shown in Fig. 10a. The compressive strength of the samples increased as the density value increased. Through observation of the data, the linear model was used to describe the relationship between the σ_c and ρ values. This linear equation expresses the relationship as follows: $\sigma_c = 85.82\rho - 104.35$. Statistical analysis showed a significant relationship between the two variables as the P-value in the analysis of variance (ANOVA) indicated that $P = 0.003$, which is lower than 0.05.[69] This equation described that one density unit 85.82 may increase the compressive strength by approximately 104.35. Additionally, the analysis of the regression coefficients (R^2) showed that this model can explain 98.67%. This means a strong relationship exists

Table 3 Microstructure and mechanical properties of the HAP–*x*CaS bone cements

x	Grain size (μm)	Compressive strength, σ_c (MPa)	Bending strength, σ_f (MPa)	Young's modulus, E (MPa)
0.3	1.29 ± 0.02	3.06 ± 0.32	1.76 ± 0.31	534.22 ± 92.14
0.4	1.26 ± 0.01	4.32 ± 0.45	2.31 ± 0.25	752.70 ± 75.11
0.5	1.22 ± 0.01	5.64 ± 0.42	3.17 ± 0.23	841.01 ± 76.01
0.6	1.20 ± 0.02	6.41 ± 0.21	4.08 ± 0.15	963.29 ± 51.72
0.7	1.19 ± 0.01	7.23 ± 0.14	4.79 ± 0.16	1097.48 ± 85.56

between these two variables.[70] Fig. 10b shows the relation of the σ_f as a function of grain size (d). The σ_f value had an exponential relation with d (first order), which can be expressed as $\sigma_f = 1.52 + 1.71 \times 10^{12} \exp -d/0.04$. The relationship between the E and porosity (P) is presented in Fig. 10c. The data distribution displayed a linear relationship between the E and P, which can be expressed as $E = 9365.75–185.72P$. This equation described that Young's modulus increased as the porosity decreased. One porosity unit of 185.72 may affect the E by approximately 9365.75. Statistical analysis showed significant correlations between the two variables. This is because the P-value in the analysis of variance is 0.001, which is lower than 0.05.[69] In addition, the regression analysis showed that this model explains 98.02% of the variability in Young's modulus.[70]

Plots of the σ_c as a function of CaS content at various incubation days from 1, 3, and 7 days of the HAP–xCaS bone cements are shown in Fig. 11. The initial compressive strength of the cement samples varied in the range of 3.06–7.23 MPa, which is in good agreement for the brushite cement.[71] The σ_c of all samples increased as the incubation day increased. After 7 days of incubation, the maximum σ_c value of 12.85 MPa was obtained for the x = 0.7 bone cement sample, which was ~77.73% higher than that of the 1 day of incubation. This also showed similar behavior observed in previous works.[72–74] Ding *et al.*[74] also found that the σ_c of the tricalcium silicate/gluconodelta-lactone/calcium sulfate dehydrate or C3S/GDL/CSD composite cement increased as the incubation time increased.

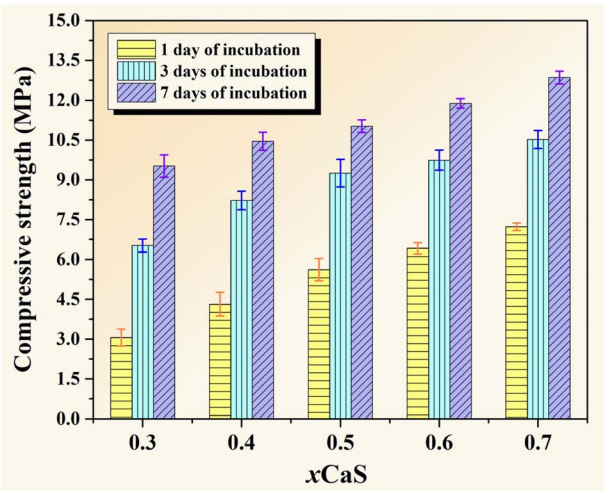

Fig. 11 Plots of σ_c at various incubation days (1, 3, and 7 days) as a function of CaS content of the HAP–xCaS bone cements.

The comparison properties of the HAP–0.7CaS bone cement for this work with other existing bone cement are shown in Table 4. It was found that the lowest setting time was obtained for the HAP–0.7CaS bone cement. Moreover, the compressive strength values (after incubation of 1 day and 7 days) of the current work are considerably high when compared with other existing bone cement.[13,57]

3.7 *In vitro* apatite-forming ability and pH behavior tests

Currently, two common methods have been used to test the *in vitro* bioactivity of the biomaterials. One method is to evaluate the apatite-formation ability in the SBF. The other method is to investigate *in vitro* bone cell response.[75] However, in this work, the apatite formation on its surface in SBF solution is used to predict the bioactivity/biocompatibility of a material.[76] Wu *et al.*[75] and Kokubo *et al.*[76] also reported that this method can be used for screening bone bioactive materials before animal testing, and the number of animals used and the duration of animal experiments can be remarkably reduced using this method, which can assist in the efficient development of new types of bioactive materials. The essential requirement for an artificial material to bond to living bone is the formation of bonelike apatite on its surface when implanted in the living body, and this *in vitro* apatite formation can be reproduced in the SBF solution with ion concentrations nearly equal to those of human blood plasma.[76–78] To confirm bioactivity, we observed apatite precipitation on the top of bone cement surfaces over a specific period after being immersed in SBF. The HAP–xCaS bone cements were limited to 1 cm^2 of the active area and were immersed in falcon tubes containing 40 mL of SBF solution at 37 °C in a water bath.[25] After 7 and 14 days of soaking in the SBF solution, the SEM technique studied each sample again. SEM micrographs of the HAP–xCaS bone cements after being soaked in SBF solution for 7 days, where x = 0.3–0.7 are shown in Fig. 12. It was found that the addition of CaS helped to improve the biocompatibility. The SEM images confirmed that the formation of apatite crystals on the surface of all bone cement samples significantly increased as the CaS content increased. At lower CaS content (x = 0.3–0.4), a few precipitated apatite crystals were observed on the surface of bone cement. However,

Table 4 Comparison the properties of the HAP–0.7CaS bone cements with other existing bone cements

Compound	Initial setting time (min)	Compressive strength (after 1 day incubation) (MPa)	Compressive strength (after 7 days incubation) (MPa)	Ref.
HAP–0.7CaS	8.04 ± 0.15	7.23 ± 0.14	12.85 ± 0.15	This work
HAP/CS/HA-Col	21.00 ± 1.20	6.69 ± 0.52	5.94 ± 1.07	57
HAP cement with 1% $NaH_2PO_4 \cdot 2H_2O$	12.00 ± 1.50	6.00	11.50	13
HAP cement with 2% $NaH_2PO_4 \cdot 2H_2O$	12.00 ± 1.50	5.00	10.00	13

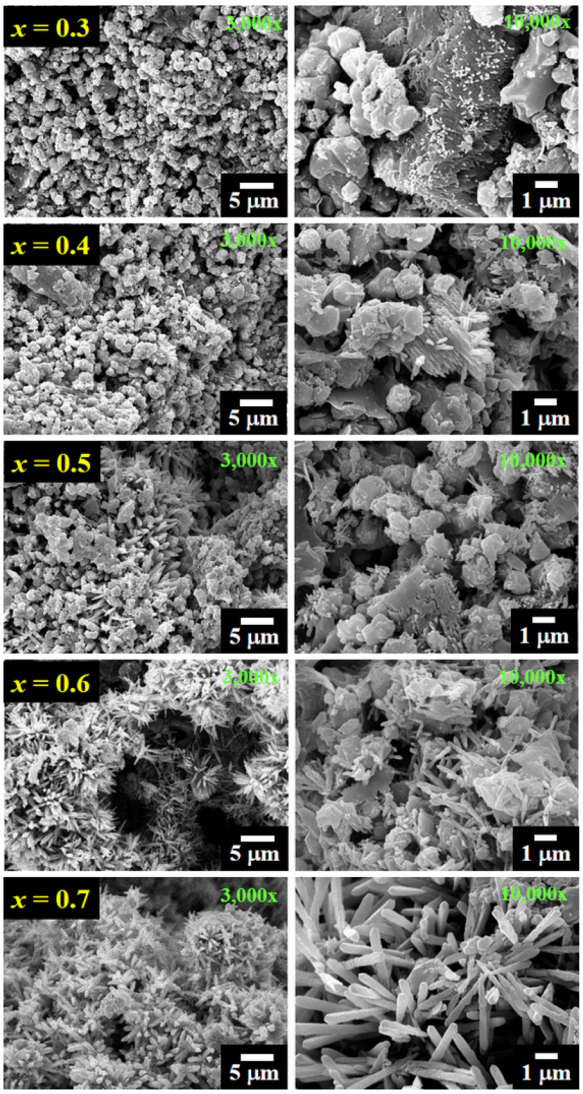

Fig. 12 SEM micrographs of the HAP–xCaS bone cements after being soaked in SBF solution for 7 days, where $x = 0.3–0.7$ and magnification of 3000× and 10 000×.

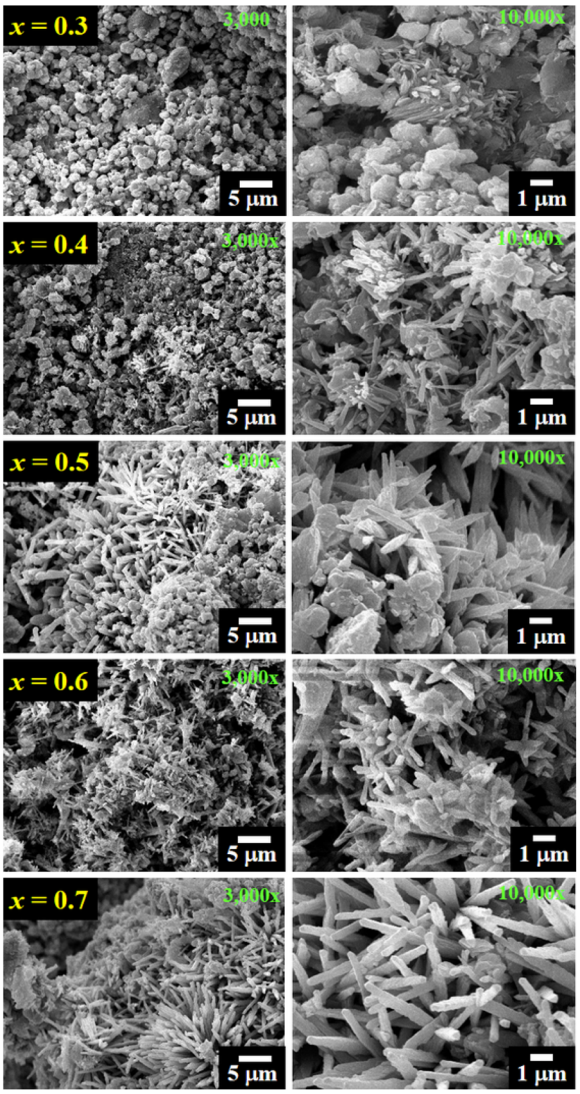

Fig. 13 SEM micrographs of the HAP–xCaS bone cements after being soaked in SBF solution for 14 days, where $x = 0.3–0.7$ and magnification of 3000× and 10 000×.

the tiny flakes of the apatite layer were more precipitated with higher added CaS content ($x = 0.5–0.6$). Notably, the apatite aggregates generally covered all the surfaces of the bone cement, especially for the $x = 0.7$ bone cement.

SEM micrographs of the HAP–xCaS bone cements after being soaked in the SBF solution for 14 days also showed a similar trend to that of 7 days of SBF immersion (Fig. 13). With a higher added amount of CaS content, the apatite layer was more precipitated and clearly observed. The tiny flakes and needle-shaped apatite layer fully covered all surface areas for the $x = 0.3–0.6$ bone cement samples. For the $x = 0.7$ bone cement sample, the apatite crystals are observed with a cylindrical shape and clump to form groups with a cactus shape. Specifically, with the sample immersed for 14 days in the SBF solution, apatite crystals grew to form a thicker block on the material's surface. Therefore, the $x = 0.7$ bone cement sample exhibited good biocompatibility in the SBF solution for this work.[79] The bioactivity of these materials was attributed to their compositional and surface characteristics.[80] Bioactive substances are brought into contact with the body's fluids, and apatite begins to form on the surface of the bone. Evidence of a chemical bond between the material and the tissue can be seen in forming an apatite layer on the contacted tissue.[75] The release of Ca^{2+} and PO_4^{3-} ions initiate apatite layer formation due to external pH changes.[29,80] Moreover, the release of Ca^{2+} and PO_4^{3-} ions plays an essential part in the tissue regeneration process.[80]

The pH changes measured over time of the HAP–xCaS bone cements containing different compositions are shown in Fig. 14. The ionic changes produced pH variation in physiological conditions.[48] After immersion in SBF solution for 3–5 days, the pH of all samples slightly decreased to around 6.7–6.9. The reason for the slight decrease in the pH value at the early stage after immersion might be attributed to the acidity of the calcium sulfate and brushite cements. However, the pH value

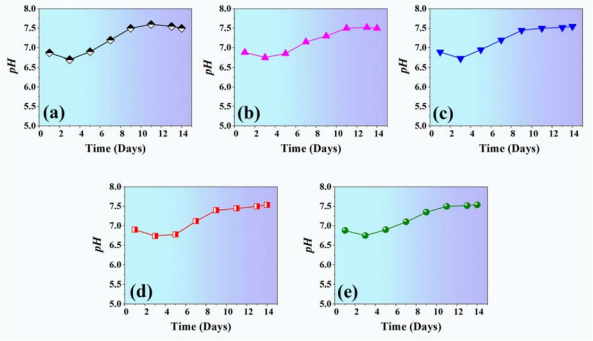

Fig. 14 Plots of pH as a function of time (days) of the HAP–xCaS bone cements containing different compositions.

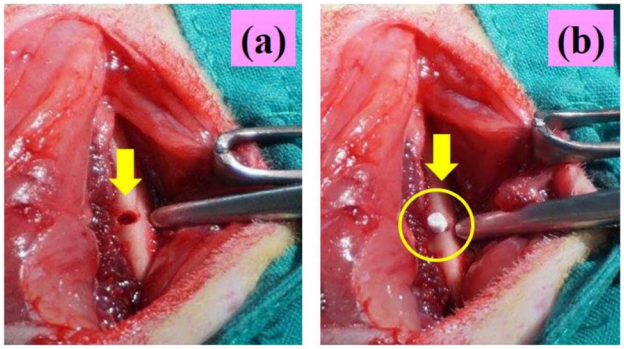

Fig. 15 Photographs of (a) the as-prepared implantation hole with a diameter of 5 mm and a depth of 10 mm on rabbit femur and (b) implantation holes filled with bone cement samples.

subsequently recovered to around 7.1–7.2 after 7 days of incubation, and the pH increased continuously to nearly 7.5 until 14 days for all compositions. Mendes *et al.*[81] also reported that the pH value in the SBF solution at 37 °C was reduced from 7.4 to around 6.0 in the first 7 days for the β-TCP/MCPM/Si bone cement. They found that this pH reduction could be attributed to the hydration reaction of brushite cements. After 7 days, the pH value gradually increased and remained constant at around 7.5. This result shows that a slight decrease in pH is not sustained and the pH is normalized to 7.5. In the context of using this material as an implant, the initial contact with fluid-buffered connective tissue may help to significantly reduce the initial pH-lowering effect so that the following pH would not have a significant effect on the human body.[48] From SEM and microstructure analysis, the study of bioactivity from pH confirmed the presence of HAP in the examined specimen,[82] and the $x = 0.7$ or HAP–0.7CaS sample exhibited better biocompatibility than other compositions.[79] The $x = 0.7$ sample also showed the highest mechanical and hardening faster than other systems. Therefore, the $x = 0.7$ composition was selected for further *in vivo* studies including implantation and histological analysis in rabbit femur (discussed in the next section).

3.8 *In vivo* results

3.8.1 Implantation of hydroxyapatite–calcium sulfate bone cement. As a result of optimization of setting time, injectability, and good mechanical properties as well as excellent *in vitro* apatite-forming ability with good biocompatibility in the SBF solution, the $x = 0.7$ (HAP–0.7CaS) composition was selected and suitable for implantation and histological analysis in rabbit femur. The $x = 0.7$ bone cement sample for implantation was formed into cylinders with a size of 5 mm in diameter × 10 mm in length and was autoclave-sterilized before implantation. Under sterile conditions, a 2.5 cm skin incision was made on each lateral femoral diaphysis with split fascia, and two implantation holes with a diameter of 5 mm and a depth of 10 mm were drilled using a trephine drill on both femoral diaphyses, as shown in Fig. 15. After placing the implantation bone cement, the fascia was sutured. The rabbits were sacrificed after 2, 4, and 8 weeks, and the femoral diaphysis was then obtained for histological analysis.

3.8.2 Histological analysis. Our experiments performed a histological evaluation of new bone formation and inflammation in the defective areas at 2, 4, and 8 weeks post-grafting HAP–0.7CaS bone cement, as shown in Fig. 16. Histological analysis is essential for evaluating the availability of biomaterials in guiding tissue regeneration and repair.[28] This technique is determined by the shape and size of macromolecules (in and around the cell), such as proteins, by sectioning, staining, and examining the sections using a microscope. It is often called microscopic anatomy. Histology allows the visualization of tissue structure and possible tissue-specific changes. A moderate new bone (NB) formation composed of trabecular bone, surrounding a central medullary cavity containing connective tissue (CT) and blood vessels, was presented in both the control and the $x = 0.7$ bone cement at 2 weeks post-implantation (Fig. 17). However, mild inflammation was also found only for 2 weeks.[49] At 4 weeks post-implantation, no inflammation, the new bone network was more developed within the femoral defect, and the newly formed bone became more mature. More new bone formed around the defect and the bone cement (BC) particles. Osteoblasts were found peripherally at the bone trabeculae, and occasional osteoblast-like cells

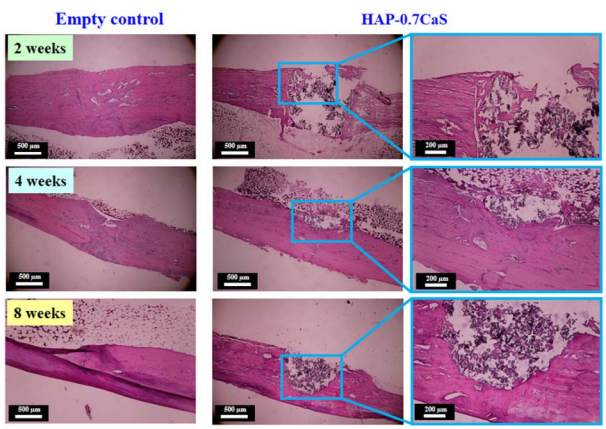

Fig. 16 Histological preparations of the HAP–0.7CaS bone cement implantation for 2, 4, and 8 weeks.

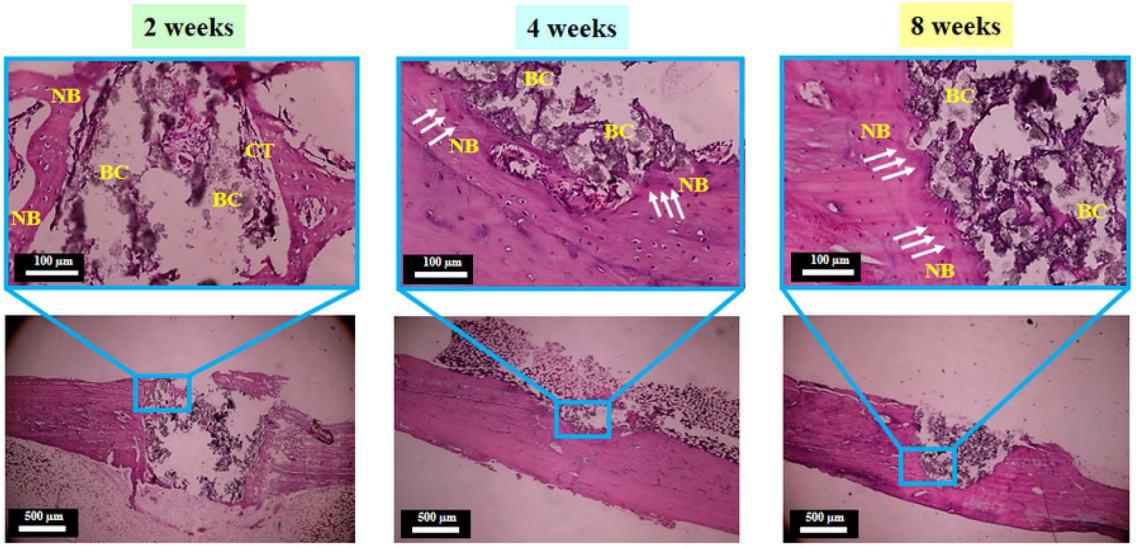

Fig. 17 Histological preparations of spontaneously healed bone defects for 2, 4, and 8 weeks of the HAP–0.7CaS bone cement. BC = bone cement, NB = new bone, and CT = connective tissue. The arrows mark the transition between the newly formed bone and the connective tissue.

were presented at the granules at 4 and 8 weeks. The histological evaluation also indicated that compatibility of the implant materials with animal tissues is acceptable because only mild inflammation was observed within and around the implant sites for 2 weeks. At 8 weeks post-implantation, a large amount of bone cement remained inside the defect area, and new bone formation was limited along the implant interface (Fig. 17). Mild periosteal fibrosis characterized by the proliferation of fibroblasts and neovascularization was shown in the control and the $x = 0.7$ bone cement group at 2 weeks, and moderate periosteal fibrosis was demonstrated in the $x = 0.7$ bone cement group at 4 weeks. However, no periosteal fibrosis was found in the control group at 4 weeks and in both the control and the $x = 0.7$ bone cement group at 8 weeks. Normally, the degradation products are continuously absorbed or excreted from the tissue as it grows in, and the repaired bone tissue completely replaces the implanted material, leaving no residual material in the body when the bone repair is completed. It has to be highlighted that a delayed or fast biodegradation rate may interfere with the rate and pattern of new bone formation.[3,83,84] For this work, the bioavailability and dissolvable properties of the CaS compound could be histologically determined by an increase in the phagocytic activity of activated macrophages surrounding the implantation sites. Moreover, activation of osteoblasts, infiltration of fibroblasts and the presence of neovascularization are the hallmarks of activated new bone formation. New bone formation was histologically observed and completely resolved at week 4 after implantation. The new bone formation results confirmed that the $x = 0.7$ (HAP–0.7CaS) bone cement had good bioactivity, supporting its use in bone repair applications.

It can be observed that the $x = 0.7$ sample had the lowest porosity, water absorption, and setting time. This composition also has the highest density and mechanical performance, hardening faster than other systems. Moreover, the $x = 0.7$ bone cement also produced a higher ability to induce *in vitro* apatite precipitation and showed good bioactivity. *In vivo* histological analysis also confirmed that the $x = 0.7$ sample exhibited good biocompatibility. Based on all the above results, this suggests that the $x = 0.7$ bone cement has the potential to be a promising material candidate for bone repair applications, *i.e.* healing bone fractures, and bone filling in clinical.

4 Conclusions

In this study, a new biomaterial of HAP–xCaS bone cements (where x = 0–1) was successfully prepared. The setting time, injectability, washout resistance tests, phase evaluation, physical properties, water absorption analysis, microstructure, mechanical properties, *in vitro* apatite-forming ability, and pH behavior of the prepared bone cements as a function of CaS added content were examined. Implantation of the $x = 0.7$ or HAP–0.7CaS bone cement and histological (*in vivo*) were also analyzed in this work. The mixed phases of HAP, CaS, brushite, and gypsum were found in the XRD pattern. The mechanical properties (σ_c, σ_f, and E) increased as the CaS content increased, which correlated with all HAP–xCaS bone cements exhibiting a dense structure. The average grain size decreased as the CaS content increased. The $x = 0.7$ bone cement also produced a higher ability to induce apatite precipitation. Histological analysis for the $x = 0.7$ bone cement found that a moderate new bone formation composed of trabecular bone, surrounding a central medullary cavity containing connective tissue (CT) and blood vessels, was presented. More new bone (NB) formed around the defect and the bone cement (BC) particles for 4–8 weeks post-implantation. Based on our results, this suggests that the $x = 0.7$ bone cement has the potential to be a promising material candidate for biomedical applications with good bioactivity, injectability, and good mechanical properties, which are essential for bone repair applications, *i.e.* healing bone fractures and filling bone defects in clinical settings.

Data availability

Data will be made available on request.

Author contributions

Pharatree Jaita: writing – original draft, methodology, investigation. Komsanti Chokethawai: review & editing. Chamnan Randorn: formal analysis, review & editing. Kittikorn Boonsri: investigation, data curation. Kidsadagon Pringproa: investigation, data curation. Kriangkrai Thongkorn: investigation, data curation. Anucha Watcharapasorn: review & editing, visualization. Parkpoom Jarupoom: writing – review & editing, conceptualization, supervision.

Conflicts of interest

There are no conflicts to declare.

Acknowledgements

This research project was supported by Fundamental Fund 2024, Chiang Mai University. This research has received funding support from the NSRF *via* the Program Management Unit for Human Resources & Institutional Development, Research and Innovation [B05F640198] and Fundamental Fund, Rajamangala University of Technology Lanna. Department of Industrial Engineering, Materials and Medical Innovation Research Unit, Materials and Manufacturing Research Center, Faculty of Engineering, Rajamangala University of Technology Lanna, Department of Physics and Materials Science, Center of Excellence in Materials Science and Technology, Materials Science Research Center, Faculty of Science, Office of Research Administration, and Center of Veterinary Diagnosis and Technology Transfer, Faculty of Veterinary Medicine, Chiang Mai University are also acknowledged.

References

1 A. Zima, J. Czechowska, D. Siek and A. Ślósarczyk, Influence of magnesium and silver ions on rheological properties of hydroxyapatite/chitosan/calcium sulphate based bone cements, *Ceram. Int.*, 2017, **43**, 16196–16203.

2 W. C. Liu, H. Y. Wang, L. C. Chen, S. W. Huang, C. Wu and R. J. Chung, Hydroxyapatite/tricalcium silicate composites cement derived from novel two-step sol-gel process with good biocompatibility and applications as bone cement and potential coating materials, *Ceram. Int.*, 2019, **45**, 5668–5679.

3 F. Hao, L. Qin, J. Liu, J. Chang, Z. Huan and L. Wu, Assessment of calcium sulfate hemihydrate-tricalcium silicate composite for bone healing in a rabbit femoral condyle model, *Mater. Sci. Eng., C*, 2018, **88**, 53–60.

4 W. Liu, D. Zhai, Z. Huan, C. Wu and J. Chang, Novel tricalcium silicate/magnesium phosphate composite bone cement having high compressive strength, *in vitro* bioactivity and cytocompatibility, *Acta Biomater.*, 2015, **21**, 217–227.

5 M. Wekwejta, N. Moritz, B. S. Żureka and A. Pałubicka, Biomechanical testing of bioactive bone cements-a comparison of the impact of modifiers: antibiotics and nanometals, *Polym. Test.*, 2018, **70**, 234–243.

6 D. Siek, A. Ślósarczyk, A. Przekora, A. Belcarz, A. Zima, G. Ginalska and J. Czechowska, Evaluation of antibacterial activity and cytocompatibility of α-TCP based bone cements with silver-doped hydroxyapatite and $CaCO_3$, *Ceram. Int.*, 2017, **43**, 13997–14007.

7 P. Feng, R. Zhao, W. Tang, F. Yang, H. Tian, S. Peng, H. Pan and C. Shuai, Structural and functional adaptive artificial bone: materials, fabrications, and properties, *Adv. Funct. Mater.*, 2023, **33**, 2214726.

8 E. Sassoni, G. Graziani, E. Franzoni and G. W. Scherer, Conversion of calcium sulfate dihydrate into calcium phosphates as a route for conservation of gypsum stuccoes and sulfated marble, *Constr. Build. Mater.*, 2018, **170**, 290–301.

9 C. Shuai, W. Yang, P. Feng, S. Peng and H. Pan, Accelerated degradation of HAP/PLLA bone scaffold by PGA blending facilitates bioactivity and osteoconductivity, *Bioact. Mater.*, 2021, **6**, 490–502.

10 C. Shuai, B. Peng, P. Feng, L. Yu, R. Lai and A. Min, *In situ* synthesis of hydroxyapatite nanorods on graphene oxide nanosheets and their reinforcement in biopolymer scaffold, *J. Adv. Res.*, 2022, **35**, 13–24.

11 A. L. Lesniewicz, P. Szczepanska, M. Kaminska, M. Nowosielska and A. S. Guzend, 6-Step manufacturing process of hydroxyapatite filler with specific properties applied for bone cement composites, *Ceram. Int.*, 2022, **48**, 26854–26864.

12 G. Furtos, M. T. Cotisel, C. Garbo, M. Senila, N. Jumate, I. V. Simiti and C. Prejmerean, New composite bone cement based on hydroxyapatite and nanosilver, *Part. Sci. Technol.*, 2013, **31**, 392–398.

13 S. M. Rabiee, F. Moztarzadeh and M. S. Hashjin, Synthesis and characterization of hydroxyapatite cement, *J. Mol. Struct.*, 2010, **969**, 172–175.

14 J. Dai, Y. Fu, D. Chen and Z. Sun, A novel and injectable strontium-containing hydroxyapatite bone cement for bone substitution: a systematic evaluation, *Mater. Sci. Eng., C*, 2021, **124**, 112052.

15 N. C. Reger, A. K. Bhargava, I. Ratha, B. Kundu and V. K. Balla, Structural and phase analysis of multi-ion doped hydroxyapatite for biomedical applications, *Ceram. Int.*, 2019, **45**, 252–263.

16 D. G. Filip, V. A. Surdu, A. V. Paduraru and E. Andronescu, Current development in biomaterials-hydroxyapatite and bioglass for applications in biomedical field: a review, *J. Funct. Biomater.*, 2022, **13**, 248.

17 W. Yu, X. Wangn, J. Zhaon, Q. Tang, M. Wang and X. Ning, Preparation and mechanical properties of reinforced hydroxyapatite bone cement with nano-ZrO_2, *Ceram. Int.*, 2015, **41**, 10600–10606.

18 M. J. Beuerlein and M. D. McKee, Calcium sulfates: what is the evidence?, *J. Orthop. Trauma*, 2010, **24**, S46–S51.
19 Y. Y. Tsai, S. F. Wang, S. T. Kuo and W. H. Tuan, Improving biodegradation behavior of calcium sulfate bone graft tablet by using water vapor treatment, *Mater. Sci. Eng., C*, 2013, **33**, 121–126.
20 W. L. Chen, C. K. Chen, J. W. Lee, Y. L. Lee, C. P. Ju and J. H. C. Lin, Structure, properties and animal study of a calcium phosphate/calcium sulfate composite cement, *Mater. Sci. Eng., C*, 2014, **37**, 60–67.
21 K. Cheng, W. Zhu, X. Weng, L. Zhang, Y. Liu, C. Han and W. Xia, Injectable tricalcium phosphate/calcium sulfate granule enhances bone repair by reversible setting reaction, *Biochem. Biophys. Res. Commun.*, 2021, **557**, 151–158.
22 Z. Cai, Z. Wu, Y. Wan, T. Yu and C. Zhou, Manipulation of the degradation behavior of calcium phosphate and calcium sulfate bone cement system by the addition of micro-nano calcium phosphate, *Ceram. Int.*, 2021, **47**, 29213–29224.
23 Z. Gu, S. Wang, W. Weng, X. Chen, L. Cao, J. Wei, J. W. Shin and J. Su, Influences of doping mesoporous magnesium silicate on water absorption, drug release, degradability, apatite-mineralization and primary cells responses to calcium sulfate based bone cements, *Mater. Sci. Eng., C*, 2017, **75**, 620–628.
24 M. Du, Q. Li, J. Chen, K. Liu and C. Song, Design and characterization of injectable abalone shell/calcium sulfate bone cement scaffold for bone defect repair, *Chem. Eng. J.*, 2021, **420**, 129866.
25 G. Yang, J. Liu, F. Li, Z. Pan, X. Ni, Y. Shen, H. Xu and Q. Huang, Bioactive calcium sulfate/magnesium phosphate cement for bone substitute applications, *Mater. Sci. Eng., C*, 2014, **35**, 70–76.
26 A. T. Moya, A. Apalimova, B. G. Navarro, R. Z. L. Gal, A. M. Roig and J. L. López, Calcium sulfate in implantology (biphasic calcium sul-fate/hydroxyapatite, BCS/HA, bond apatite®): review of the literature and case reports, *Coatings*, 2022, **12**, 1350.
27 W. J. Liu, C. T. Wu, W. N. Liu, W. Y. Zhai and J. Chang, The effect of plaster ($CaSO_4 \cdot 1/2H_2O$) on the compressive strength, self-setting property, and *in vitro* bioactivity of silicate-based bone cement, *J. Biomed. Mater. Res., Part B*, 2013, **101B**, 279–286.
28 C. C. Chen, C. W. Wang, N. S. Hsueh and S. J. Ding, Improvement of *in vitro* physicochemical properties and osteogenic activity of calcium sulfate cement for bone repair by dicalcium silicate, *J. Alloys Compd.*, 2014, **585**, 25–31.
29 A. Zima, Z. Paszkiewicz, D. Siek, J. Czechowska and A. Ślósarczyk, Study on the new bone cement based on calcium sulfate and Mg, CO_3 doped hydroxyapatite, *Ceram. Int.*, 2012, **38**, 4935–4942.
30 Z. Chen, L. Kang, Q. Y. Meng, H. Liu, Z. Wang, Z. Guo and F. Z. Cui, Degradability of injectable calcium sulfate/mineralized collagen-based bone repair material and its effect on bone tissue regeneration, *Mater. Sci. Eng., C*, 2014, **45**, 94–102.
31 M. V. Cabaňas, L. M. R. Lorenzo and M. V. Regí, Setting behavior and *in vitro* bioactivity of hydroxyapatite/calcium sulfate cements, *Chem. Mater.*, 2002, **14**, 3550–3555.
32 G. Yang, J. Liu, F. Li, Z. Pan, Xi. Ni, Y. Shen, H. Xu and Q. Huang, Bioactive calcium sulfate/magnesium phosphate cement for bone substitute applications, *Mater. Sci. Eng., C*, 2014, **35**, 70–76.
33 H. Chang, H. Xiang, Z. Yao, S. Yang, M. Tu, X. Zhang and B. Yu, Strontium-substituted calcium sulfate hemihydrate/hydroxyapatite scaffold enhances bone regeneration by recruiting bone mesenchymal stromal cells, *J. Biomater. Appl.*, 2020, **35**, 97–107.
34 T. Ma, J. Liao, Y. Zhang, J. Feng, Y. Yang, H. Li, W. Guo and J. Chen, Study on modification of hydroxyapatite/magnesium phosphate bone cement by N-acetyl-L-cysteine, *Ceram. Int.*, 2023, **49**, 16545–16553.
35 A. Asti, G. Gastaldi, R. Dorati, E. Saino, B. Conti, L. Visai and F. Benazzo, Stem cells grown in osteogenic medium on PLGA, PLGA/HA, and titanium scaffolds for surgical applications, *Bioinorg. Chem. Appl.*, 2010, **2010**, 831031.
36 P. Jarupoom and P. Jaita, Influence of barium hexaferrite on magnetic properties of hydroxyapatite ceramics, *J. Nanosci. Nanotechnol.*, 2015, **15**, 9217–9221.
37 M. P. Chang, Y. C. Tsung, H. C. Hsu, W. H. Tuan and P. L. Lai, Addition of a small amount of glass to improve the degradation behavior of calcium sulfate bioceramic, *Ceram. Int.*, 2015, **41**, 1155–1162.
38 Z. Pei, Z. Zhang, G. Li, F. Fu, K. Zhang, Y. Cai and Y. Yang, Improvement of *in vitro* osteogenesis and antimicrobial activity of injectable brushite for bone repair by incorporating with Se-loaded calcium phosphate, *Ceram. Int.*, 2021, **47**, 11144–11155.
39 W. Zhou, Y. Xue, X. Ji, G. Yin, N. Zhang and Y. Ren, A novel injectable and degradable calcium phosphate/calcium sulfate bone cement, *Afr. J. Biotechnol.*, 2011, **10**, 19449–19457.
40 W. Zhao, J. Chang and W. Zhai, Self-setting properties and *in vitro* bioactivity of $Ca_3SiO_5/CaSO_4 \cdot 1/2H_2O$ composite cement, *J. Biomed. Mater. Res.*, 2008, **85A**, 336–344.
41 P. Jaita and P. Jarupoom, Temperature dependence on structure, mechanical and electrical properties of bismuth lanthanum sodium titanate-modified lead zirconate titanate ceramics, *ScienceAsia*, 2020, **46S**, 51–57.
42 P. Jaita and P. Jarupoom, Enhanced magnetic performance and *in vitro* apatite-forming ability of the $CoFe_2O_4$ doped nano-hydroxyapatite porous bioceramics, *Microsc. Res. Tech.*, 2023, **86**, 882–897.
43 Y. M. Soon, K. H. Shin, Y. H. Koh, J. H. Lee, W. Y. Choi and H. E. Kim, Fabrication and compressive strength of porous hydroxyapatite scaffolds with a functionally graded core/shell structure, *J. Eur. Ceram. Soc.*, 2011, **31**, 13–18.
44 A. Vahdat, B. Ghasemi and M. Yousefpour, Mechanical properties of the hydroxyapatite and magnetic nanocomposite of hydroxyapatite adsorbents, *S. Afr. J. Chem. Eng.*, 2020, **33**, 90–94.

45 C. Shuai, X. Shi, K. Wang, Y. Gu, F. Yang and P. Feng, Ag-doped CNT/HAP nanohybrids in a PLLA bone scaffold show significant antibacterial activity, *Bio-Des. Manuf.*, 2024, **7**, 105–120.

46 Y. Wang, Z. Feng, X. Liu, C. Yang, R. Gao, W. Liu, W. O. Yang, A. Dong, C. Zhang, P. Huang and W. Wang, Titanium alloy composited with dual-cytokine releasing polysaccharide hydrogel to enhance osseointegration *via* osteogenic and macrophage polarization signaling pathways, *Regener. Biomater.*, 2022, **9**, rbac003.

47 A. Oyane, K. Onuma, A. Ito, H. M. Kim, T. Kokubo and T. Nakamura, Formation and growth of clusters in conventional and new kinds of simulated body fluids, *J. Biomed. Mater. Res., Part A*, 2003, **64A**, 339–348.

48 H. J. Lee, B. Kim, A. R. Padalhin and B. T. Lee, Incorporation of chitosan-alginate complex into injectable calcium phosphate cement system as a bone graft material, *Mater. Sci. Eng., C*, 2019, **94**, 385–392.

49 P. K. Ross, J. Hadzik, J. Seeliger, K. Kozak, K. Jurczyszyn, H. Gerber, M. Dominiak and C. K. Keil, New nano-hydroxyapatite in bone defect regeneration: a histological study in rats, *Ann. Anat.*, 2017, **213**, 83–90.

50 A. S. Hammood, S. S. Hassan, M. T. Alkhafagy and H. L. Jaber, Effect of calcination temperature on characterization of natural hydroxyapatite prepared from carp fish bones, *SN Appl. Sci.*, 2019, **1**, 436.

51 S. Mondal, M. E. D. A. Reyes and U. Pal, Plasmon induced enhanced photocatalytic activity of gold loaded hydroxyapatite nanoparticles for methylene blue degradation under visible light, *RSC Adv.*, 2017, **7**, 8633–8645.

52 M. S. Raita, S. L. Iconaru, A. Groza, C. Cimpeanu, G. Predoi, L. Ghegoiu, M. L. Badea, M. C. Chifiriuc, L. Marutescu, R. Trusca, C. F. Furnaris, C. S. Turculet, D. V. Enache and D. Predoi, Multifunctional hydroxyapatite coated with arthemisia absinthium composites, *Molecules*, 2020, **25**, 413.

53 D. Predoi, S. L. Iconaru, S. C. Ciobanu, S. A. Predoi, N. Buton, C. Megier and M. Beuran, Development of iron-doped hydroxyapatite coatings, *Coatings*, 2021, **11**, 186.

54 M. A. Moncea, P. A. Maria, G. Deak and G. Poteras, Binder microstructures developed during the hydration process in the system portland cement-calcium aluminate cement-calcium sulfate, *Mater. Res. Soc. Symp. Proc.*, 2016, **1812**, 71–76.

55 Z. Huan, J. Chang and X. H. Huang, Self-setting properties and *in vitro* bioactivity of $Ca_2SiO_4/CaSO_4 \cdot 1/2H_2O$ composite bone cement, *J. Biomed. Mater. Res., Part B*, 2008, **87**, 387–394.

56 S. V. Dorozhkin, Self-setting calcium orthophosphate formulations, *J. Funct. Biomater.*, 2013, **4**, 209–311.

57 S. Subramaniam, Y. H. Fang, S. Sivasubramanian, F. H. Lin and C. P. Lin, Hydroxyapatite-calcium sulfate-hyaluronic acid composite encapsulated with collagenase as bone substitute for alveolar bone regeneration, *Biomaterials*, 2016, **74**, 99–108.

58 O. D. Oguz, A. R. Boccaccini and D. Loca, Injectable bone cements: what benefits the combination of calcium phosphates and bioactive glasses could bring?, *Bioact. Mater.*, 2023, **19**, 217–236.

59 Z. Chen, H. Liu, X. Liu, X. Lian, Z. Guo, H. J. Jiang and F. Z. Cui, Improved workability of injectable calcium sulfate bone cement by regulation of self-setting properties, *Mater. Sci. Eng., C*, 2013, **33**, 1048–1053.

60 J. Zhang, W. Liu, V. Schnitzler, F. Tancret and J. M. Bouler, Calcium phosphate cements for bone substitution: chemistry, handling and mechanical properties, *Acta Biomater.*, 2014, **10**, 1035–1049.

61 R. O'Neill, H. O. McCarthy, E. B. Montufar, M. P. Ginebra, D. I. Wilson, A. Lennon and N. Dunne, Critical review: injectability of calcium phosphate pastes and cements, *Acta Biomater.*, 2017, **50**, 1–9.

62 A. Ferreira, C. Oliveira and F. Rocha, The different phases in the precipitation of dicalcium phosphate dehydrate, *J. Cryst. Growth*, 2003, **252**, 599–611.

63 S. Ucar, S. H. Bjørnøy, D. C. Bassett, B. L. Strand, P. Sikorski and J. P. Andreassen, Transformation of brushite to hydroxyapatite and effects of alginate additives, *J. Cryst. Growth*, 2017, **468**, 774–778.

64 V. V. Smirnov, O. S. Antonova, M. A. Goldberg, S. V. Smirnov, L. I. Shvorneva, A. A. Egorov, A. S. Baikin and S. M. Barinov, Bone cements in the calcium phosphate-calcium sulfate system, *Dokl. Chem.*, 2016, **467**, 136–139.

65 D. Nagrockienė, A. Rutkauskas, I. Pundienė and I. Girnienė, The effect of silica fume addition on the resistance of concrete to alkali silica reaction, *IOP Conf. Ser.: Mater. Sci. Eng.*, 2019, **660**, 012031.

66 O. A. Osuchukwu, A. Salihi, I. Abdullahi, B. Abdulkareem and C. S. Nwannenna, Synthesis techniques, characterization and mechanical properties of natural derived hydroxyapatite scaffolds for bone implants: a review, *SN Appl. Sci.*, 2021, **3**, 822.

67 P. Jaita and P. Jarupoom, Enhanced dielectric, piezoelectric, and mechanical performances of barium strontium titanate-modified $(Bi_{0.487}Na_{0.487}La_{0.017})TiO_3$ lead-free ceramics, *Integr. Ferroelectr.*, 2021, **213**, 209–220.

68 O. G. C. Pineda, W. H. Kao, M. I. L. Bastarrachea, Y. V. Pantoja, J. V. C. Rodríguez and J. M. C. Uc, Towards optimization of the silanization process of hydroxyapatite for its use in bone cement formulations, *Mater. Sci. Eng., C*, 2014, **40**, 157–163.

69 T. Arahira, M. Maruta and S. Matsuya, Characterization and *in vitro* evaluation of biphasic α-tricalcium phosphate/β-tricalcium phosphate cement, *Mater. Sci. Eng., C*, 2017, **74**, 478–484.

70 S. A. A. Tajudin, M. A. M. Azmi, S. Shahidan, M. H. Z. Abidin and A. Madun, Relationship of physical parameters in Pb-contaminated by stabilization/solidification method, *MATEC Web Conf.*, 2016, **47**, 03015.

71 M. Roy, K. DeVoe, A. Bandyopadhyay and S. Bose, Mechanical and *in vitro* biocompatibility of brushite cement modified by polyethylene glycol, *Mater. Sci. Eng., C*, 2012, **32**, 2145–2152.

72 W. Liu, C. Wu, W. Liu, W. Zhai and J. Chang, The effect of plaster $(CaSO_4 \cdot 1/2H_2O)$ on the compressive strength, self-

setting property, and *in vitro* bioactivity of silicate-based bone cement, *J. Biomed. Mater. Res., Part B*, 2013, **101B**, 279–286.

73 Q. Fu, N. Zhou, W. Huang, D. Wang, L. Zhang and H. Li, Preparation and characterization of a novel bioactive bone cement: glass based nanoscale hydroxyapatite bone cement, *J. Mater. Sci.: Mater. Med.*, 2004, **15**, 1333–1338.

74 Z. Ding, W. Xi, M. Ji, H. Chen, Q. Zhang and Y. Yan, Developing a biodegradable tricalcium silicate/gluconodelta-lactone/calcium sulfate dihydrate composite cement with high preliminary mechanical property for bone filling, *Mater. Sci. Eng., C*, 2021, **119**, 111621.

75 C. Wu and Y. Xiao, Evaluation of the *in vitro* bioactivity of bioceramics, *Bone Tissue Regener. Insights*, 2009, **2**, 25–29.

76 T. Kokubo and H. Takadama, How useful is SBF in predicting *in vivo* bone bioactivity?, *Biomaterials*, 2006, **27**, 2907–2915.

77 A. J. Jose and M. Alagar, Preparation and characterization of polysulfone-based nanocomposites, *Manufacturing of nanocomposites with engineering plastics*, 2015, pp. 31–59.

78 D. K. Pattanayak, S. Yamaguchi, T. Matsushita, T. Nakamura and T. Kokubo, Apatite-forming ability of titanium in terms of pH of the exposed solution, *J. R. Soc., Interface*, 2012, **9**, 2145–2155.

79 T. M. T. Dinh, T. T. Nguyen, T. N. Pham, T. P. Nguyen, T. T. T. Nguyen, T. Hoang, D. Grossin, G. Bertrand and C. Drouet, Electrodeposition of HAp coatings on Ti_6Al_4V alloy and its electrochemical behavior in simulated body fluid solution, *Adv. Nat. Sci.: Nanosci. Nanotechnol.*, 2016, **7**, 025008.

80 A. Cahyanto, M. Liemidia, E. Karlina, M. N. Zakaria, K. A. Shariff, C. Sukotjo and A. E. Ghannam, Bioactive carbonate apatite cement with enhanced compressive strength *via* incorporation of silica calcium phosphate composites and calcium hydroxide, *Materials*, 2023, **16**, 2071.

81 L. S. Mendes, S. Saska, F. Coelho, T. S. O. Capote, R. M. S. Caminaga, R. Marchetto, R. G. Carrodeguas, A. M. M. Gaspar and M. A. Rodríguez, Injectable β-TCP/MCPM cement associated with mesoporous silica for bone regeneration: characterization and toxicity evaluation, *Biomed. Mater.*, 2018, **13**, 025023.

82 R. Fada, M. Shahgholi and M. Karimian, Improving the mechanical properties of strontium nitrate doped dicalcium phosphate cement nanoparticles for bone repair application, *Ceram. Int.*, 2021, **47**, 14151–14159.

83 D. Liu, C. Cui, W. Chen, J. Shi, B. Li and S. Chen, Biodegradable cements for bone regeneration, *J. Funct. Biomater.*, 2023, **14**, 134.

84 M. Ebrahimi, M. G. Botelho and S. V. Dorozhkin, Biphasic calcium phosphates bioceramics (HA/TCP): concept, physicochemical properties and the impact of standardization of study protocols in biomaterials research, *Mater. Sci. Eng., C*, 2017, **71**, 1293–1312.